Towards an *ab initio* theory for the temperature dependence of electric field gradients in solids: Application to hexagonal lattices of Zn and Cd

A. V. Nikolaev ●

Skobeltsyn Institute of Nuclear Physics Lomonosov Moscow State University, 119991 Moscow, Russia;
School of Electronics, Photonics and Molecular Physics, Moscow Institute of Physics and Technology, 141700,
Dolgoprudny, Moscow Region, Russia;
and National Research Nuclear University MEPhI, 115409, Kashirskoe shosse 31, Moscow, Russia

N. M. Chtchelkatchev ●

Vereshchagin Institute for High Pressure Physics, Russian Academy of Sciences, 108840 Troitsk, Moscow, Russia;
Ural Federal University, 620002, Ekaterinburg, Russia;
and Moscow Institute of Physics and Technology, 141700 Dolgoprudny, Moscow Region, Russia

D. A. Salamatin

Vereshchagin Institute for High Pressure Physics, RAS, 142190 Troitsk, Moscow, Russia
and Dzelepov Laboratory of Nuclear Problems, Joint Institute for Nuclear Research, 141980 Dubna, Russia

A. V. Tsvyashchenko

Vereshchagin Institute for High Pressure Physics, RAS, 142190 Troitsk, Moscow, Russia

Based on *ab initio* band-structure calculations we formulate a general theoretical method for description of the temperature dependence of an electric-field gradient in solids. The method employs a procedure of averaging multipole electron-density component ($l \neq 0$) inside a sphere vibrating with the nucleus at its center. As a result of averaging, each Fourier component ($K \neq 0$) on the sphere is effectively reduced by the square root of the Debye-Waller factor [$\exp(-W)$]. The electric-field gradient related to a sum of K components most frequently decreases with temperature (T), but under certain conditions because of the interplay between terms of opposite signs, it can also increase with T. The method is applied to calculations of the temperature evolution of the electric-field gradients of pristine zinc and cadmium crystallized in the hexagonal lattice. For calculations within our model, of crucial importance is the temperature dependence of mean-square displacements which can be taken from experiment or obtained from the phonon modes in the harmonic approximation. For the case of Zn, we have used data obtained from single-crystal x-ray diffraction. In addition, for Zn and Cd, we have calculated mean-square displacements with the density-functional perturbation treatment of the QUANTUM ESPRESSO package. With the experimental data for displacements in Zn, our calculations reproduce the temperature dependence of the electric-field gradient very accurately. Within the harmonic approximation of the QUANTUM ESPRESSO package, the decrease in electric-field gradients in Zn and Cd with temperature is overestimated. Our calculations indicate that the anharmonic effects are of considerable importance in the temperature dependence of electric-field gradients.

I. INTRODUCTION

The electric-field gradient (EFG) is a very sensitive characteristic of electron structure [1–4]. It is directly measured by the family of methods experiencing quadrupole hyperfine interactions, such as nuclear quadrupole resonance, Mössbauer spectroscopy, and perturbed angular correlation (PAC) spectroscopy [4–6]. Nuclear probes in these techniques are exposed to the local electronic and molecular structures via the electric interaction between the nuclear quadrupole moment and the surrounding electronic charge distribution providing a spectroscopic fingerprint of the electron environment.

The methods are utilized in a wide range of applications. The time-differential perturbed γ-γ angular correlation (TDPAC) spectroscopy [5,6], for example, can be used in biochemistry characterizing interactions between metal ions and proteins [7], point defects in metals, and, recently, in semiconductors [8] and surface and interface properties, detecting charge-density wave formations and structural phase transitions [9] in various materials. Although the TDPAC spectroscopy has been known for more than 40 years, it still has a rich potential for solid-state physics and novel materials [6–8].

On the other hand, the EFGs measured by these techniques can be confronted with theoretical values obtained from *ab initio* calculations [10–12] which should give a thorough picture of microscopic properties of the investigated material.

Recently, such a comparison has led to an improved value of the nuclear quadrupole moment of cadmium [13,14]. The problem is, however, that, in many cases, there is a strong temperature (T) dependence of the EFGs [1–3,15], discussed in detail in Sec. II A below, which is often not taken into account. In contrast to *ab initio* calculations of the EFGs, first-principles studies of the T dependence of theEFGs are very rare [2,16]. Several models put forward in the past (see Sec. II A) rely heavily on phenomenological parameters [1,3].

In the present paper, following the *ab initio* path, we formulate a theoretical approach to this problem, which on the basis of crucial band-structure parameters [17] can describe the T evolution (i.e., decrease or increase) of the EFG in detail. We demonstrate our method by applying it to the hexagonal-close-packed (hcp) structure of zinc and cadmium both of which show the characteristic temperature decrease in the EFG [1,18].

The paper is written as follows: in Sec. II, we give details of our approach, in Sec. III, we describe our results for the T reduction of the EFG in hcp zinc and cadmium, discussing separately the possibility of the *increasing* EFG with T in Sec. III C. Our conclusions are summarized in Sec. IV.

II. THEORETICAL MODEL

A. Theoretical background and models of the T dependence

The EFG tensor V_{ij} is defined as the second partial spatial derivatives of an electric self-consistent-field potential V evaluated at the nuclear site, i.e.,

$$V_{ij} = \frac{\partial^2 V}{\partial i \, \partial j}, \tag{1}$$

where $i = x, y, z$. Since V_{ij} is a symmetric (traceless) second rank tensor, it can be further diagonalized by transforming coordinates to the principal system of axes where $|V_{zz}| \geqslant |V_{yy}| \geqslant |V_{xx}|$. (Thus, the number of independent parameters for the EFG in the principal axis system is reduced to two.) The principal component (V_{zz}) is called the electric-field gradient, and the second independent parameter is the asymmetry η defined as $\eta = (V_{xx} - V_{yy})/V_{zz}$ ($0 \leqslant \eta \leqslant 1$).

Very often, EFGs demonstrate a strong temperature (T) dependence which can be described by a equation of this form

$$V_{zz}(T) = V_{zz}(T = 0)(1 - BT^\alpha), \tag{2}$$

where the coefficient $B > 0$ implying a smaller EFG with increasing T and the coefficient α is usually $3/2$ [18,19]. Later, however, this "universal" form of the T dependence was corrected [20]: It was attributed to normal (sp) metals, whereas for transition metals, deviations from the $T^{3/2}$ law were notable (down to $\alpha \approx 1$). In some cases, the quadratic approximation, also gave good quality fits [20]. Even in classical systems, such as ^{67}Zn in zinc metal or ^{111}Cd probes in cadmium metal, there were found deviations from the $T^{3/2}$ law at low temperatures [20].

Since the discovery of strong T dependence of the EFG, the problem has been considered theoretically [16,22–26]. Two main approaches have been put forward in the past: One is based on electron band-structure methods [22,23,25,26], whereas the other used screened charged potential formalism

[24]. A starting point for both methods is, in fact, the phenomenological expression for V_{zz} [27],

$$V_{zz} = (1 - \gamma_\infty)V_{zz}^{\text{latt}} + (1 - R)V_{zz}^{el}, \tag{3}$$

where V_{zz}^{latt} is the field gradient due to the noncubic arrangement of ions in the lattice (excluding the central site), corrected by the antishielding factor γ_∞ and V_{zz}^{el} is due to the conduction electrons corrected by the shielding factor R [1]. The screened charged method works with V_{zz}^{latt} calculating lattice sums over vibrating ions, whereas the first approach works with the electron contribution (V_{zz}^{el}) and considers V_{zz}^{latt} as virtually temperature independent. Nowadays, however, we do not analyze the EFG in terms of V_{zz}^{latt}, V_{zz}^{el}, γ_∞, and R. With the success of *ab initio* all-electron methods for the electronic structure of solids [10–12] capable of treating the electron potential of general shape, the electric-field gradient V_{zz} at zero temperature can be found directly from the obtained self-consistent potential. Equation (3) then should be rewritten in a general form as

$$V_{zz} = V_{zz}^{\text{out}} + V_{zz}^{\text{in}}, \tag{4}$$

where V_{zz}^{in} is the local contribution due to the EFG, for example, from the charges inside a muffin-tin (MT) sphere, whereas V_{zz}^{out} is from the charges outside the MT sphere [more details on Eq. (4) are given below in Sec. II C]. Moreover, V_{zz}^{in} and V_{zz}^{out} can be calculated, and we know that, by far, the leading term is V_{zz}^{in} [16]. In our case, $V_{zz}^{\text{out}}/V_{zz}$ amounts only to -2.7% for Zn and -1.1% for Cd. (The minus sign of V_{zz}^{out} is discussed in Ref. [3].)

In Ref. [22], Jena started with V_{zz}^{in} and used reduced matrix elements $M' = M \exp(-W)$ of the pseudopotential which appeared as a result of averaging M over the lattice vibrations [28]. Note that $\exp(-W)$ is a square root of the Debye-Waller factor (SRDWF) $\exp(-2W)$. Keeping in $\exp(-W) \approx 1 - W$ only the first-order term in $W \ll 1$, he finally arrived at

$$V_{zz} = V_{zz}(0)[1 - \beta\varphi(T/T_D)]. \tag{5}$$

Here, T_D is an effective Debye temperature, the function φ is the Debye integral [29], and β is an adjustable constant. Since at low T, $\varphi(T/T_D)$ approaches the zero-point value as T^2, and at high T, increases linearly with T, in the region of $0 < T/T_D < 2$, a $T^{3/2}$ behavior is approximately followed. The concept of Ref. [22] continued in a number of publications on the T dependence of the EFG [23,25,26]. These studies cannot be attributed to a true *ab initio* approach, although elements of it are present in Refs. [26,28]. Although the T curves for V_{zz} can be reproduced in some cases, one should be aware that, in Eq. (5), T_D and especially β are fitting parameters of the model. Explicit EFG computation in these models has been avoided in favor of finding expected trends with temperature.

Nowadays, although we can successfully obtain the $T = 0$ value of V_{zz} by performing *ab initio* band-structure calculations, the problem of finding its T dependence from first principles remains. It is a difficult and laborious problem because it requires an accurate calculation of both electronic and phonon properties. Probably, the first attempt was performed by Torumba *et al.* in Ref. [16], who used molecular dynamics and a supercell calculation of pristine cadmium. For the T dependence of V_{zz} atoms in the supercell were displaced

according to the values of mean-square displacements at this temperature after which the value of $V_{zz}(T)$ was obtained by averaging over various displacive configurations. The authors have observed the decrease in the EFG with T in the supercell approach, although their data deviate from the experimental curve at $T > 500$ K.

Surprisingly, in some studies, an increase in V_{zz} with T has been reported. For example, in 5% Fe-doped In_2O_3 [30], in the rutile modification of TiO_2 [31,32] and in tetrahedrally coordinated Fe sites in $Bi_2(Fe_xGa_{1-x})_4O_9$ [15]. In the rutile structure, the situation is, in fact, probe dependent: Whereas the EFG measured at ^{47,49}Ti or substitutional ^{181}Ta and ^{44}Sc increases with T, it changes in the opposite direction for ^{111}Cd probes [31,32]. The increase in the EFG is in disagreement with the classical treatment [33,34] of the evolution of the EFG in ionic and molecular crystals based on small rotations of the gradient tensor with respect to a fixed system of axes, according to which

$$\langle V_{zz}\rangle = V_{zz}(0)\left[1 - \frac{3}{2}\left(\langle\theta_x^2\rangle + \langle\theta_y^2\rangle\right)\right]. \quad (6)$$

Here, θ_x and θ_y are small rotations about the x and y axes, respectively, and $\langle\theta_x\rangle = \langle\theta_y\rangle = 0$. Note that Eq. (6) always leads to a decrease in the EFG with T.

Below, we formulate a theoretical approach to this problem, which, depending on specific conditions, can result both in temperature decrease or increase of the EFG with temperature. It establishes a close relation between the values of the mean-square displacements and the evolution of the EFG and uses the square root of the Debye-Waller factor $\exp(-W)$ which lies at the center of early phenomenological models [1,22,24]. The method is applied to the temperature decrease in V_{zz} in hcp zinc and cadmium [1,18].

B. Reduced quadrupole potential and density on the displaced MT spheres

The temperature dependence of the EFG is clearly a manifestation of both electron and phonon properties. To evaluate correctly V_{zz}, we have to effectively average it over atomic vibrations because a typical frequency of the lattice vibrations (1 THz = 10^{12} Hz) is large compared to a typical quadrupole frequency (100 MHz = 10^8 Hz) experienced by nuclear probes in solids.

The electron density of a solid $\rho(\vec{R})$ is a translationally invariant quantity,

$$\rho(\vec{R} + \vec{a}_i) = \rho(\vec{R}), \quad (7)$$

where $\vec{a}_i$ ($i = 1$–3) are the basis vectors of the Bravais lattice. Therefore, $\rho(\vec{R})$ can be expanded in Fourier series,

$$\rho(\vec{R}) = \sum_{\vec{K}} \rho(\vec{K})e^{i\vec{K}\cdot\vec{R}}, \quad (8)$$

where the vectors $\vec{K}$ belong to the reciprocal lattice. Fourier components $\rho(\vec{K})$ are usually found quite naturally from solutions of the Schrödinger (or Dirac) equation for an electron in a periodic mean-field potential of the solid. According to the Bloch theorem, the solution for the electron band j has the
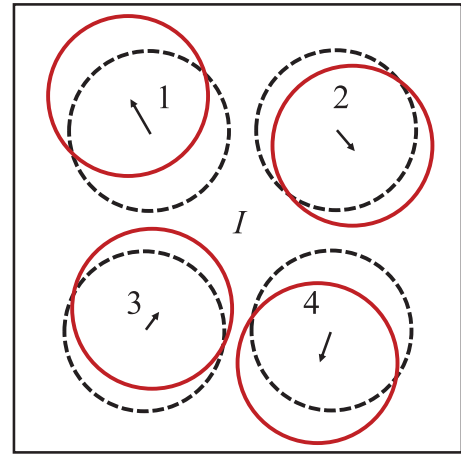

FIG. 1. Vibrations of MT-spheres $n = 1$–4 and the interstitial region (I). The dashed lines: averaged surfaces positions in the ideal structure; the full (red) lines: instantaneous positions; the arrows indicate the sphere displacements u_n, $n = 1$–4. As a result of sphere vibrations, the averaged quadrupole potential $\langle V_Q\rangle$ on the sphere surfaces is reduced, see the text for details.

form

$$\Psi_{\vec{k},j}(\vec{R}) = \sum_{\vec{K}} c_{\vec{k},j}(\vec{K})\phi_{\vec{K}+\vec{k}}(\vec{R}), \quad (9)$$

where the vector $\vec{k}$ lies in the first Brillouin zone, $\phi_{\vec{K}+\vec{k}}$'s are basis functions, and $c_{\vec{k},j}(\vec{K})$'s are the coefficients of expansion in the basis set. Almost in all computational methods, the basis functions are modified plane waves, which, in the interstitial region, are simply $\phi_{\vec{K}+\vec{k}}(\vec{R}) \sim \exp[i(\vec{K}+\vec{k})\cdot\vec{R}]$. Substituting Eq. (9) in

$$\rho(\vec{R}) = 2 \sum_{\vec{k},j:E(\vec{k},j)\leqslant E_F} |\Psi_{\vec{k},j}(\vec{R})|^2, \quad (10)$$

where E_F is the Fermi energy, we obtain Eq. (8) with the Fourier coefficients $\rho(\vec{K})$ given by

$$\rho(\vec{K}) = \sum_{\vec{k},j:E(\vec{k},j)\leqslant E_F} \sum_{\vec{K}'} c^*_{\vec{k},j}(\vec{K}')c_{\vec{k},j}(\vec{K}'+\vec{K}). \quad (11)$$

The electron density in the interstitial region is only weakly dependent on the amplitudes of the vibrations since the band electron on average experiences a periodic potential from the regular arrangement of the ions. On the other hand, the electron density around a nucleus being attached to it by the Coulomb interaction is expected to follow adiabatically the vibrating ion. To reconcile these apparently contradictory viewpoints, we consider a model of vibrating spheres [called below muffin-tin or MT spheres], Fig. 1, which are immersed in the crystal. We keep the values of $\rho(\vec{K})$, Eq. (11) in the interstitial region unchanged whereas the electron density on the vibrating sphere will be calculated taking into account the nuclear displacements. It turns out that, at a finite and even zero temperature T, the quantities $\rho(\vec{K})$ on vibrating MT spheres are effectively reduced (see below). In the language of the linearized augmented plane-wave (LAPW) method, this implies a modification of boundary conditions for the solutions inside the MT sphere [35], which, in turn, changes the

EFG. Therefore, our main goal is to calculate the temperature dependence of the electron density on the vibrating sphere, which later (Sec. II D) will be used for the calculation of the EFG. In the following, we consider a simple case of a single atom in the primitive unit cell. (This avoids unnecessary technical complications, whereas the generalization for the case of few atoms is straightforward.)

The electron density on a MT sphere of the radius R_{MT} centered at a site n and displaced from the equilibrium position $\vec{X}(n) = \{X_x(n), X_y(n), X_z(n)\}$ by the vector $\vec{u}_n$ can be expanded in the multipole series,

$$\rho(\vec{u}_n, r = R_{MT}, \theta, \phi) = \sum_\Lambda \rho_\Lambda(\vec{u}_n) S_\Lambda(\theta, \phi), \quad (12)$$

where $\Lambda \equiv (l, \tau)$ stands for A_{1g} irreducible representations of the crystal point group, $S_\Lambda(\theta, \phi)$'s are corresponding symmetry adapted functions (SAFs), l is the multipole orbital index, and τ counts functions with the same l (if there are few such functions). The polar angles $\Omega = (\theta, \phi)$ are specified by the vector $\vec{r}$ from the nuclear position ($\vec{X} + \vec{u}$). $S_\Lambda(\theta, \phi)$'s are linear combinations of real spherical harmonics ($Y_l^{m,c} \sim \cos m\phi$ and $Y_l^{m,s} \sim \sin m\phi$) defined by the crystal site symmetry and tabulated in Ref. [36]. The first function with $\Lambda = 0$ ($l = 0$, $\tau = 1$) is the spherically symmetric (monopole) contribution $S_0 = Y_{l=0}^{m=0} = 1/\sqrt{4\pi}$. For the hexagonal close-packed structure defined by the basis vectors specified in Ref. [36], the other multipole functions are as follows: $Y_{l=2}^{m=0}$, $Y_{l=3}^{3,c}$, $Y_{l=4}^{m=0}$, $Y_{l=5}^{3,c}$, $Y_{l=6}^{m=0}$, $Y_{l=6}^{6,c}$, etc. The index Λ runs over $(0, 1) \equiv 0$, $(2, 1) \equiv Q$, $(3,1)$, $(4,1)$, $(5,1)$, $(6,1)$, $(6,2)$, etc. Thus, we have only one quadrupolar function $S_Q \equiv S_{l=2} = Y_{l=2}^{m=0}$, which explicitly reads as

$$S_Q(z) = \frac{1}{4}\sqrt{\frac{5}{\pi}}(3z^2 - 1), \quad (13)$$

where $z = \cos\theta$. Then, the general equation (12) can be written as

$$\rho(\vec{u}, \theta, \phi) = \frac{\rho_0(\vec{u})}{\sqrt{4\pi}} + \rho_Q(\vec{u}) S_Q(\theta, \phi)$$
$$+ \rho_{(3,1)}(\vec{u}) Y_{l=3}^{3,c}(\theta, \phi) + \cdots. \quad (14)$$

Rewriting the plane-wave expansion in spherical harmonics (e.g., Eq. (34.3) of Ref. [37]) in the complete basis set of symmetry adapted spherical harmonics (Eq. (2.4) of Ref. [38]), one can obtain the expansion in terms of SAFs centered at the displaced nucleus of the site n given by $\vec{X}(n) + \vec{u}_n$,

$$e^{i\vec{K}\cdot\vec{R}} = e^{i\vec{K}(\vec{X}(n)+\vec{u}_n)} 4\pi$$
$$\times \sum_\Lambda i^l j_l[Kr(n)] S_\Lambda(\hat{K}) S_\Lambda[\theta(n), \phi(n)]. \quad (15)$$

Here, j_l's are spherical Bessel functions and $\hat{K}$ specifies the direction of $\vec{K}$, i.e., $\hat{K} \equiv (\theta_{\vec{K}}, \phi_{\vec{K}})$. From Eq. (8), then, we obtain for the coefficients ρ_Λ, Eqs. (12) and (14), at any chosen site n,

$$\rho_\Lambda(\vec{u}) = 4\pi i^l \sum_{\vec{K}} j_l(KR_{MT}) S_\Lambda(\hat{K}) \rho_{\vec{u}}(\vec{K}), \quad (16)$$

where $\vec{u} \equiv \vec{u}_n$ and

$$\rho_{\vec{u}}(\vec{K}) = e^{i\vec{K}\cdot\vec{u}} \rho(\vec{K}). \quad (17)$$

Here, we have taken into account that for vectors $\vec{K}$ and $\vec{X}(n)$ belonging to the reciprocal and direct lattice, respectively, $e^{i\vec{K}\vec{X}} = 1$. In the case of $\vec{u} = 0$ (i.e., at the equilibrium position $\vec{X}$), we get $\rho_{\vec{u}}(\vec{K}) = \rho(\vec{K})$, where $\rho(\vec{K})$ is defined by Eq. (11). Averaging over the displacements at the chosen site n, we arrive at

$$\langle\rho_\Lambda\rangle = \langle\rho_\Lambda(\vec{u})\rangle = 4\pi i^l \sum_{\vec{K}} j_l(KR_{MT}) S_\Lambda(\hat{K}) \langle\rho(\vec{K})\rangle, \quad (18)$$

where

$$\langle\rho(\vec{K})\rangle = \langle e^{i\vec{K}\cdot\vec{u}}\rangle \rho(\vec{K}). \quad (19)$$

Note that Eqs. (18) and (19) are independent of n because the thermal averages $\langle\rho(\vec{K})\rangle \equiv \langle\rho_{\vec{u}_n}(\vec{K})\rangle$ and $\langle\exp(i\vec{K}\cdot\vec{u}_n)\rangle$ are the same for all equivalent atoms. As has been proved by Glauber [39], the thermal average on the right-hand side of Eq. (19) can be transformed to

$$\langle e^{i\vec{K}\cdot\vec{u}}\rangle = e^{-W(\vec{K},T)}, \quad (20)$$

where

$$W(\vec{K}, T) = \frac{1}{2}\langle(\vec{K}\cdot u)^2\rangle. \quad (21)$$

Since the usual Debye-Waller factor is $\exp(-2W)$ [29], the temperature function $\exp(-W)$, Eq. (20), is the SRDWF. Such a function has been used by Kasowski for the description of the temperature-dependent Knight shift in cadmium [28]. The function W can also be written in k space [29] in the familiar form

$$W(\vec{K}, T) = \frac{1}{2N} \sum_{\vec{k},s} \langle[\vec{K}\cdot u_s(\vec{k})]^2\rangle, \quad (22)$$

where the summation runs over all vectors $\vec{k}$ in the first Brillouin zone and the phonon branches s, whereas $u_s(\vec{k})$ stands for the corresponding phonon amplitudes. From space symmetry considerations, it follows that the function $W(\vec{K})$ is the same for a set of (nonequivalent) vectors (rays) $\vec{K}_i$ obtained from $\vec{K}_1 = \vec{K}$ by the application to $\vec{K}_1$ all rotational or mirror symmetry elements of the crystal point group (i.e., for the vectors $\vec{K}_i$ belonging to the same star). In the harmonic approximation, W implicitly depends on the temperature through the number of thermally excited phonons $n_{\vec{K},s}$. In the Debye approximation at high temperatures, $(T \gg T_D)$ $W \sim T$.

For the calculation of the EFG, we need the quadrupole component $\Lambda = (2, 1)$] of the electron density and potential, the Appendix. For that purpose, with the final expressions (18)–(21), we obtain for the average quadrupole component $\langle\rho_Q\rangle$ of density on the MT sphere in Eq. (14),

$$\langle\rho_Q\rangle = -4\pi \sum_{\vec{K}} j_2(KR_{MT}) S_Q(\hat{K}) e^{-W(\vec{K},T)} \rho(\vec{K}). \quad (23)$$

This expression will be used later in Sec. II D.

Since for all $\vec{K} \neq 0$, we have $W(\vec{K}) > 0$ even for zero temperature, the corresponding averaged Fourier components $\langle\rho(\vec{K})\rangle$ in Eqs. (18) and (19) are effectively reduced. The

reduction means that, as a rule, the quadrupole component [$\langle \rho_Q \rangle$ in Eq. (14)] and the other components with $\Lambda' > 0$ (i.e., $\langle \rho_{(3,1)} \rangle$, etc.) on the MT-sphere surface are decreased in absolute value in comparison with their static values: $|\langle \rho_{\Lambda'}(\vec{u}) \rangle| < |\rho_{\Lambda'}(\vec{u} = 0)|$. As will be discussed below in Sec. II D, the effective decrease in $\langle \rho_Q \rangle$ occurs also in the interior of the MT-sphere $r \leqslant R_{MT}$ and finally leads to a reduction of the EFG. In some rare cases as a result of the interplay between terms of opposite signs in Eq. (23), an increase in $\langle \rho_Q \rangle$ can occur. Such a situation is discussed in detail below in Sec. III C.

The reduction or increase in $\langle \rho_Q \rangle$, however, does not affect the total charge of the sphere because the integral over the polar angles for SAFs S_Q, $Y_3^{3,c}$, and the others with $l \neq 0$ are zero. The total charge of the sphere is due to the monopole term ($l = 0$), which is closely related to the $\vec{K} = 0$ term in the Fourier expansion of density, Eq. (8). Note that the $\rho(K = 0)$ component is independent of T, Eq. (19), keeping the total charge inside the sphere approximately constant. A very small decrease in the average value of $\langle \rho_0 \rangle$ in Eq. (14) (implying a small increase in the charge in the interstitial region) can be accounted for by a small increase in the $\rho(K = 0)$ component of the Fourier expansion (8). In our calculations, the effect is found small and has been neglected.

In the following, we will apply our approach to the case of the hexagonal-close-packed structure, although, in principle, the consideration is general and can be used for other noncubic lattices.

C. The EFG and quadrupole ($L = 2$) expansion of the electron potential around the nucleus

In this section, we demonstrate that the reduction (or increase) in $\langle \rho_Q \rangle$ inside the MT sphere results in a corresponding change in the quadrupole component of the potential and the electric-field gradient.

Similar to the density expansion Eq. (12), the electron self-consistent-field Coulomb potential of the general form around a nucleus, employed, for example, in the full potential linearized augmented plane-wave (FLAPW) method [35,40], also can be expanded in multipolar series,

$$V(r, \theta, \phi) = \sum_\Lambda V_\Lambda(r) S_\Lambda(\theta, \phi). \tag{24}$$

Note that the coefficients $V_\Lambda(r)$ for the potential and $\rho_\Lambda(r)$ for electron-density Eq. (12) can be obtained from *ab initio* electron band-structure calculations. In Figs. 2 and 3, we reproduce such dependencies for the quadrupole component $l = 2$.

From a scrupulous analysis of the multipolar components of the potential (see the Appendix and Ref. [38]), it follows that, in the neighborhood of the nucleus (when $r \ll 1$), the radial dependence of the function $V_{l,\tau}$ reads as

$$V_\Lambda(r) = v_\Lambda r^l, \tag{25}$$

where v_Λ is a constant. This, in particular, implies that, for quadrupolar component [$\Lambda = (2, 1)$], we have $V_Q \equiv V_{(2,1)}(r) = v_Q r^2$ for the component $\Lambda = (4, 1)$ $V_{(4,1)}(r) = v_{(4,1)}r^4$, etc. This dependence of $V_Q(r)$ is illustrated in Fig. 3. It is worth noting that the quadrupolar electron-density
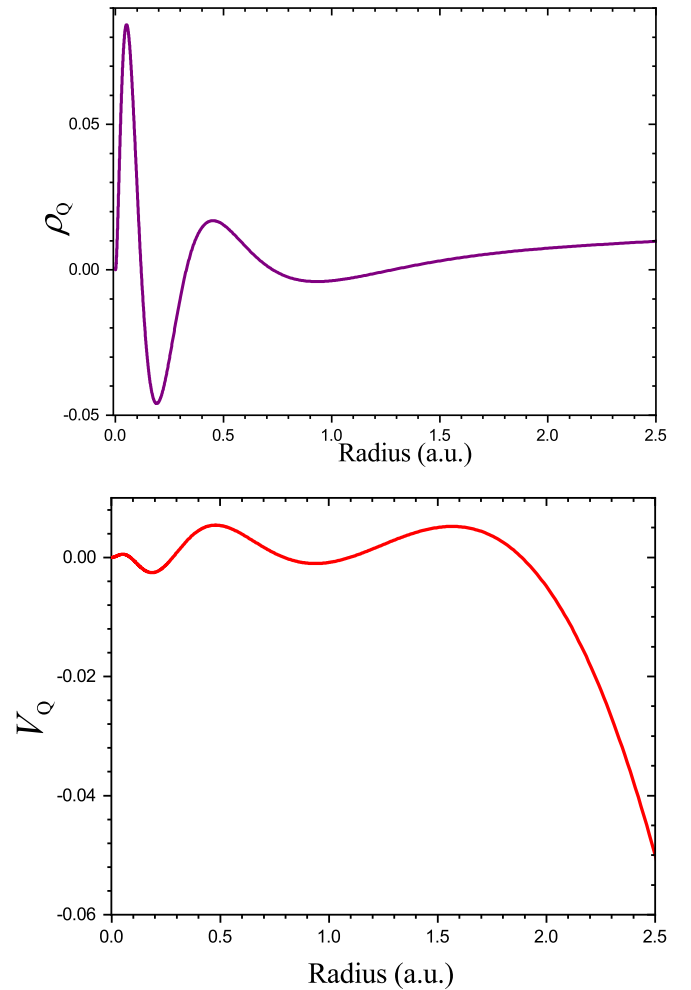

FIG. 2. Density functional theory (DFT) calculation of the quadrupole ($l = 2$) component $\rho_Q(r)$ of electron density (top panel) and the corresponding Coulomb potential $V_Q(r)$ (bottom panel) inside the MT sphere of the hcp structure of Zn ($a = 2.659$, $c = 4.851$, $R_{MT} = 1.33$ Å, or 2.51 a.u.).

component also follows the same law close to the nucleus, i.e., $\rho_Q(r) \propto r^2$, Fig. 3.

Taking Eq. (25) into account, we obtain for the electric-field gradient,

$$V_{zz} = \frac{\partial^2 V_Q}{\partial z^2} = \sqrt{\frac{5}{\pi}} v_Q. \tag{26}$$

Details are given in the Appendix. Note that Eq. (26) gives a temperature-independent EFG.

The quadrupole potential on the MT-sphere V_Q^S consists of two contributions,

$$V_Q^S = V_Q^{S,\text{out}} + V_Q^{S,\text{in}}. \tag{27}$$

Here, $V_Q^{S,\text{out}}$ and $V_Q^{S,\text{in}}$ are the potentials due to all charges outside the MT sphere and inside it, respectively. Correspondingly, for the quadrupole potential V_Q at any point $\vec{r} = (r, \theta, \phi)$ inside the MT sphere, we have

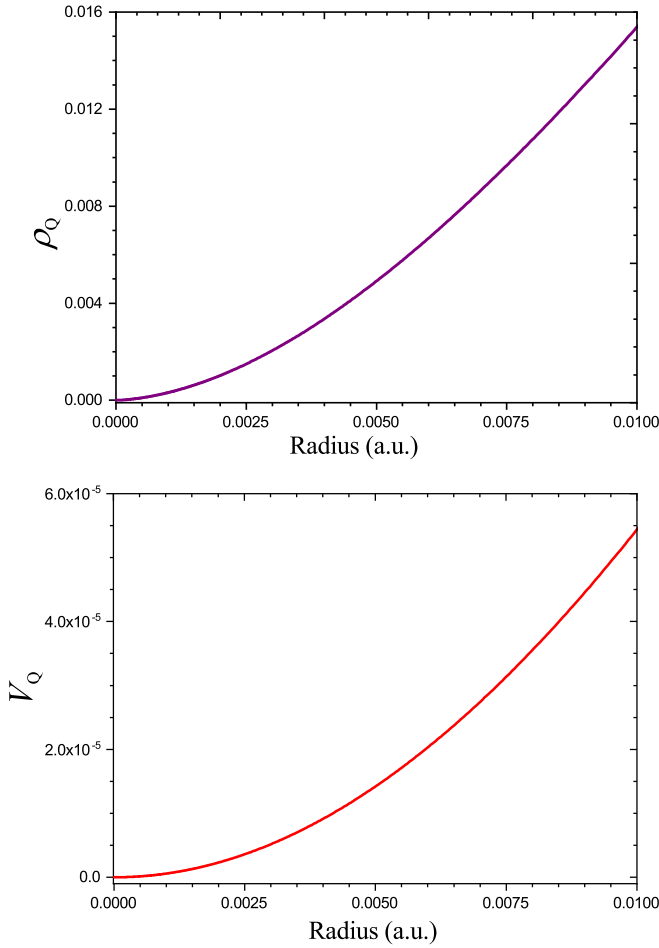$$V_Q(\vec{r}) = V_Q^{\text{out}}(\vec{r}) + V_Q^{\text{in}}(\vec{r}), \tag{28a}$$

FIG. 3. DFT calculation of the quadrupole ($l = 2$) component $\rho_Q(r)$ of electron density (top panel) and the corresponding Coulomb potential $V_Q(r)$ (bottom panel) of the hcp structure of Zn in the vicinity of the nucleus. (Fig. 2 zoomed at $r = 0$.) Both the density and the potential are proportional to r^2. For comparison, the Zn nuclear radius is 9.1×10^{-5} a.u.

where

$$V_Q^{\text{out}}(r, \theta, \phi) = V_Q^{S,\text{out}} \frac{r^2}{R_{\text{MT}}^2} S_Q(\theta, \phi), \qquad (28b)$$

(for hcp lattices $S_Q = Y_2^0$) and

$$V_Q^{\text{in}}(r, \theta, \phi) = \frac{4\pi}{5} \left(\frac{q_Q(r)}{r^3} + r^2 q_Q'(r) \right) S_Q(\theta, \phi). \quad (28c)$$

Here,

$$q_Q(r) = \int_0^r \rho_Q(r') r'^3 dr', \qquad (29a)$$

$$q_Q'(r) = \int_r^{R_{\text{MT}}} \frac{\rho_Q(r')}{r'} dr'. \qquad (29b)$$

Since $q_Q'(R_{\text{MT}}) = 0$, we find $V_Q^{S,\text{in}} = 4\pi q(R_{\text{MT}})/R_{\text{MT}}^3$. Note that V_Q^{out} is explicitly proportional to r^2, Eq. (28b). It can be shown [38] that the same holds for V_Q^{in} at $r \ll 1$. From

Eqs. (25) and (26), we then arrive at

$$V_{zz} = \sqrt{\frac{5}{\pi}} \left(v_Q^{\text{out}} + v_Q^{\text{in}} \right). \qquad (30)$$

Here, v_Q^{out} and v_Q^{in} are obtained from V_Q^{out}/r^2 and V_Q^{in}/r^2 when $r \to 0$. As a result of the reduction of $\langle \rho_Q(r) \rangle$ with temperature, $\langle v_Q^{\text{out}} \rangle$ and $\langle v_Q^{\text{in}} \rangle$ also become reduced, and $\langle V_{zz} \rangle$ decreases with temperature.

D. Temperature dependence of the EFG

As shown in Sec. II B, the average quadrupole density component $\langle \rho_Q(R_{\text{MT}}) \rangle$ on the vibrating MT sphere as a rule is reduced, Eq. (23). However, to calculate exactly the effect of the reduction on EFG, we have to know $\langle \rho_Q(r) \rangle$ at all values of $r \leqslant R_{\text{MT}}$, see Sec. II C. In a straightforward approach, we should perform a calculation for $\langle \rho_Q(r) \rangle$ inside the MT sphere considering the new value of $\langle \rho_Q(R_{\text{MT}}) \rangle$, Eq. (23) as an input boundary condition. In practice, by changing R_{MT} in a range close to the maximal (contact) radius R_{max}, we have found that the reduction of the quadrupolar density component $\rho_Q(r, T)/\rho_Q(r, T = 0)$ is approximately constant. In Zn, for example, the change in R_{MT} from the R_{max} value of 2.517 to 2.30 a.u. at 300 K results in a change in the ratio from 0.945 to 0.926 (2%). We, then, in a first approximation, assume that, for all $r \leqslant R_{\text{MT}}$,

$$\frac{\rho_Q(r, T)}{\rho_Q(r, T = 0)} = \frac{\rho_Q(R_{\text{MT}}, T)}{\rho_Q(R_{\text{MT}}, T = 0)} = R^{\text{in}}(T). \qquad (31)$$

According to Eqs. (29a) and (29b), the reduced quadrupolar density component $\langle \rho_Q(r, T) \rangle$ for all $r \leqslant R_{\text{MT}}$ changes the quadrupole charges as $q_Q(r, T) = R^{\text{in}}(T) q_Q(r)$ and $q_Q'(r, T) = R^{\text{in}}(T) q_Q'(r)$. This, in turn, leads to the reduction of $V_Q^{\text{in}}(T) = R^{\text{in}}(T) V_Q^{\text{in}}$, Eq. (28c), and $v_{(2,0)}^{\text{in}}(T) = R^{\text{in}}(T) v_{(2,0)}^{\text{in}}$. We, then, for the temperature evolution of the EFG, have

$$V_{zz}(T) = \sqrt{\frac{5}{\pi}} \left[R^{\text{out}}(T) v_{(2,0)}^{\text{out}} + R^{\text{in}}(T) v_{(2,0)}^{\text{in}} \right] \qquad (32)$$

[compare with Eq. (30)]. Here, the factor $R^{\text{out}}(T)$ accounts for the change in the potential due to all charges outside the MT sphere, whereas $v_{(2,0)}^{\text{out}}$ and $v_{(2,0)}^{\text{in}}$ are temperature independent (calculated with an *ab initio* electron band-structure method). In practice, $v_{(2,0)}^{\text{out}}$ is found to be small (1–3%) compared to $v_{(2,0)}^{\text{in}}$. Since in addition, the difference between R^{out} and R^{in} is not essential, in the following, for simplicity, we take $R^{\text{out}} \approx R^{\text{in}}$. Then, the temperature dependence of the EFG is completely due to the change in ρ_Q inside the MT sphere and

$$V_{zz}(T) \approx R^{\text{in}}(T) V_{zz}. \qquad (33)$$

Equations (33) and (31) imply that we consider the change in the quadrupole interaction as a perturbation causing a linear effect inside the MT sphere.

E. Mean-square displacements

The SRDW factor, Eqs. (20) and (21), depends crucially on the mean-square displacements $\langle u_x^2 \rangle$, $\langle u_y^2 \rangle$, and $\langle u_z^2 \rangle$, which are functions of temperature. For the hcp lattice $\langle u_x^2 \rangle = \langle u_y^2 \rangle$,
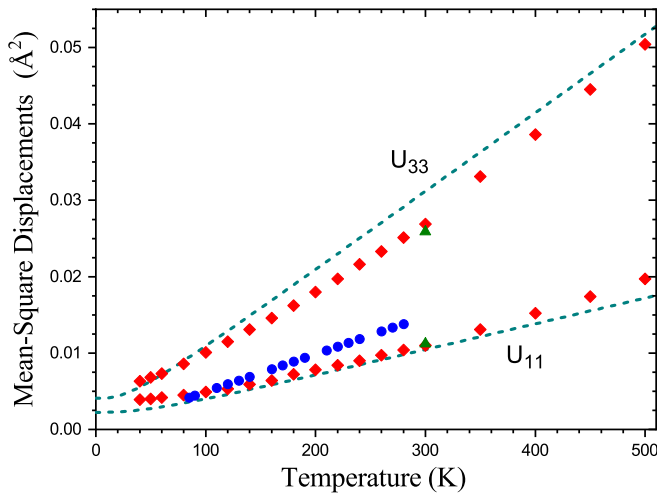
FIG. 4. Temperature evolution of $U_{11} = \langle u_x^2 \rangle$ and $U_{33} = \langle u_z^2 \rangle$ for hcp Zn found by various methods. The dark cyan dashed lines stand for calculations in the harmonic approximation (density-functional perturbation theory (DFPT) of QUANTUM ESPRESSO (QE) [41,42]), the red diamonds are experimental data from the single-crystal structural refinement of Zn at different T's [21], the olive triangles are experimental data at $T = 300$ K [43], and the blue circles are obtained from experimentally determined phonon density of states [44].

and for calculations of SRDWF, we need to know only two functions: $U_{11}(T) = \langle u_x^2 \rangle$ and $U_{33}(T) = \langle u_z^2 \rangle$ (for the hcp lattice $U_{33} > U_{11}$),

$$W(\vec{K}, T) = \tfrac{1}{2} \left[\left(K_x^2 + K_y^2 \right) U_{11}(T) + K_z^2 U_{33}(T) \right]. \quad (34)$$

The functions $U_{11}(T)$ and $U_{33}(T)$ can be calculated within the harmonic approximation or extracted experimentally as illustrated in Fig. 4 for the hcp lattice of Zn.

In Fig. 5, we plot individual SRDW factors $\exp[-W(\vec{K}, T)]$ for the hcp structure of Zn, which are responsible for the temperature reduction of the quadrupole density and potential, Sec. II B. With the increase in T, the SRDW factors get shifted to lower values. A finite width of SRDWF for reciprocal vectors with close values of $|\vec{K}|$ is due to different orientations of $\vec{K}$ with respect to the ellipsoid of mean-square displacements. The width becomes larger with the increase in asymmetry between U_{11} and U_{33}.

III. APPLICATION TO ZINC AND CADMIUM

In this section, we apply the method described earlier to calculations of the temperature dependence of the electric-field gradient of solid zinc and cadmium crystallized in the hexagonal close-packed lattice.

For that, we need data on the Fourier expansion of the electron density in the interstitial region, quadrupole components of electron density, and the potential obtained from the electron band-structure calculations. Electron density-functional calculations have been performed with the MOSCOW-FLAPW code [17]. The code explicitly takes into account the nuclear size and the change in the potential and the wave function inside the nuclear region to obtain the electric-field gradient accurately. In addition, the number of radial points inside
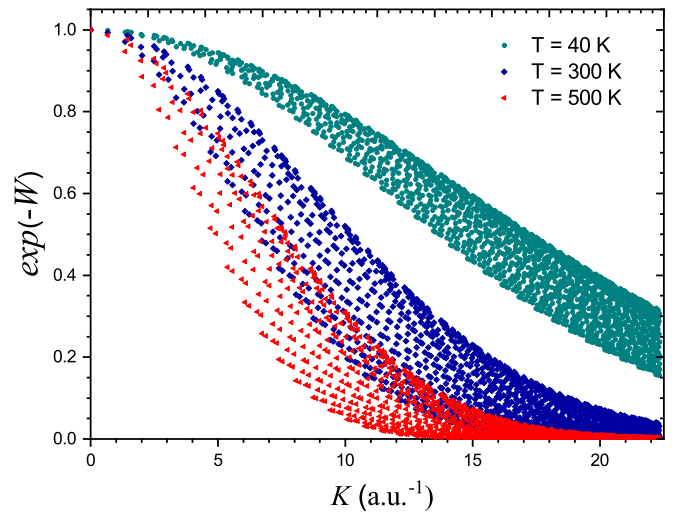

FIG. 5. SRDWFs $\exp[-W(\vec{K}, T)]$ as functions of the modulus of reciprocal vectors $K = |\vec{K}|$ of hcp Zn for various temperatures. The dark cyan circles are data for $T = 40$ K; the blue squares: $T = 300$ K; and the red triangles: $T = 500$ K. Calculations are based on experimental data for the mean-square displacements $U_{11}(T)$ and $U_{33}(T)$, Ref. [21].

the MT region has been increased to 3000 (for some runs 3500). The typical LAPW basis set cutoff parameter was $R_{MT} K_{max} = 9$ (the number of basis functions was 221), the number of k points was 704 (1331), and the maximal value of the LAPW plane-wave expansion was $l_{max} = 10$. We have used the tetrahedron method for the linear interpolation of energy between k points [45]. For calculation of the exchange-correlation potential and the exchange-correlation energy contribution, we have used the Perdew-Burke-Ernzerhof (PBE) variant [46] of the generalized-gradient approximation within the DFT at experimental lattice constants at room temperature [$a = 2.663$, $c = 4.944$, $R_{MT} = 1.196$ Å (Zn), and $a = 2.996$, $c = 5.674$, $R_{MT} = 1.429$ Å (Cd)].

Also, the temperature evolution of the tensor of mean-square displacements, $U_{11}(T)$ and $U_{33}(T)$, is required for the calculation of the square root of the Debye-Waller factor, $\exp[-W(\vec{K}, T)]$ for vectors $\vec{K}$ of the reciprocal lattice, Eqs. (34) and (20). The temperature evolution of the tensor of mean-square displacements can be obtained by three different ways: (1) from a direct experimental parametrization of the displacements $\langle u_x^2(T) \rangle$ and $\langle u_z^2(T) \rangle$ as given in Ref. [21] for Zn; (2) from calculations of the phonon frequencies and eigenvectors (for example, within the DF perturbation treatment of lattice dynamics with QUANTUM ESPRESSO [41,42]); (3) from effective Debye temperature $T_D(T)$ which appears as a result of experimental parametrization [44,47]. The strict harmonic approximation is adopted only in (2), whereas, in (1) and (3), anharmonic effects, such as thermal expansion of solids and phonon softening are effectively taken into account. Experimentally, the values of $\langle u_x^2(T) \rangle$ and $\langle u_z^2(T) \rangle$ (or directly related to them temperature factors $B_x(T)$ and $B_z(T)$ [44]) are found from the temperature evolution of the x-ray-diffraction spectra.

For the phonon part (2) of the calculations, the first-principles pseudopotential method as implemented in the QE
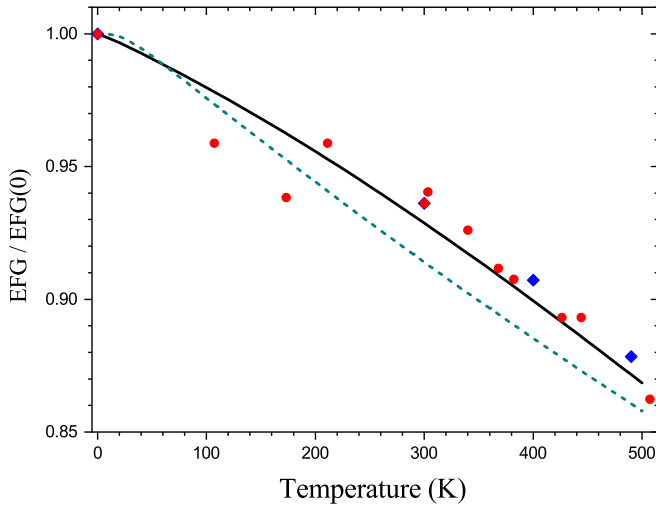
FIG. 6. Temperature dependence of the electric-field gradient in Zn, $V_{zz}(T)/V_{zz}(T=0)$. Calculations—solid black line—are based on experimental data for the mean-square displacements $U_{11}(T)$ and $U_{33}(T)$, Ref. [21]. DFPT-QE calculations [41,42]—dark cyan dashed line—have been performed in the harmonic approximation. The red circles [18] and blue diamonds [50] stand for experimental data on the EFG ratios.

package [41,42] with the PBE exchange-correlation functional [46] has been employed. The projected-augmented-wave-type scalar-relativistic pseudopotentials have been taken from the standard solid-state pseudopotential library [48,49]. The integration over the Brillouin zone for the electron density of states has been performed on a $24 \times 24 \times 12$ grid of k points, and the plane-wave kinetic cutoff energy was 70 Ry. The lattice-dynamical calculations have been carried out within the DFPT. Phonon dispersions have been computed using the interatomic force constants based on a $6 \times 6 \times 4$ k-point grid with a $48 \times 48 \times 24$ grid used to obtain the phonon densities of states and $U_{11}(T)$ and $U_{33}(T)$.

A. Zinc

Mean-square displacements for the hcp structure of zinc are shown in Fig. 4. First, we note that, in the DFPT-QE harmonic approximation in the region of T from 60 to 500 K, $U_{11}(T)$ and $U_{33}(T)$ are practically linear in T. Such behavior is also expected in the Debye model for $T > T_D$. Experimentally, however, we observe that $U_{11}(T)$ and $U_{33}(T)$ deviate from the linear law. As shown in Ref. [21], $U_{11}(T)$ and $U_{33}(T)$ are approximated by quadratic functions of T for all data in the range from 40 to 500 K. In addition, in the harmonic approximation values of U_{33} are slightly overestimated, Fig. 4, which results in a considerable suppression of the SRDW factors and the calculated temperature dependence of the EFGs, Fig. 6. On the other hand, our calculations of the temperature evolution of the EFG using experimental data for $U_{11}(T)$ and $U_{33}(T)$ demonstrate a good correspondence with the measured values of V_{zz}, Fig. 6. We have also found that the T dependence of V_{zz} is extremely sensitive to the ratio $\mathcal{R} = U_{33}/U_{11}$. To demonstrate it, we have computed the evolution of V_{zz} with T with reduced values of $\mathcal{R}$, Fig. 7
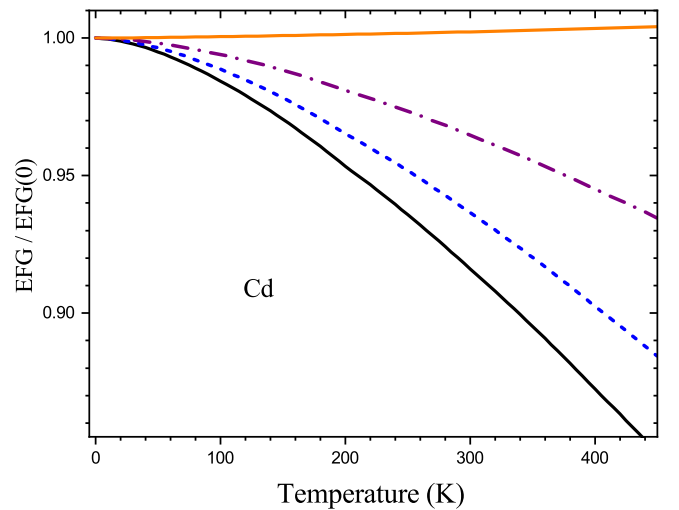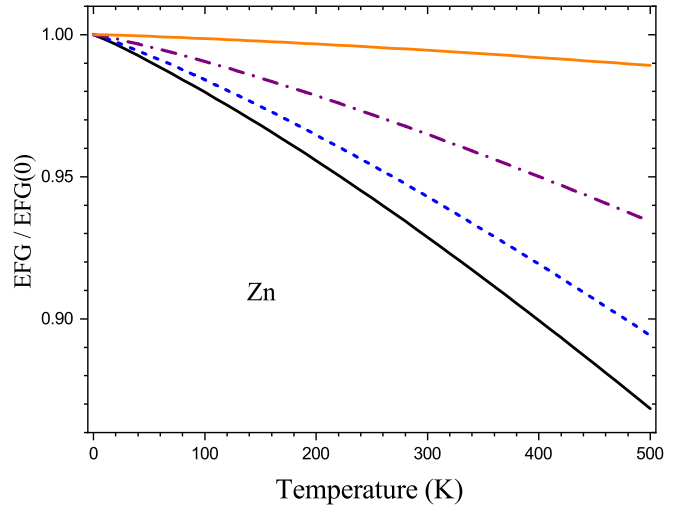

FIG. 7. Evolution of the T dependence of V_{zz} with a reduction of the mean-square displacement ratio $\mathcal{R} = U_{33}/U_{11}$ whereas keeping the averaged value of the displacements U_{av}, Eq. (35), unchanged. The black solid line corresponds to the initial value of $\mathcal{R}_0 = U_{33}/U_{11}$, the others—to reduced $\mathcal{R}$. The blue dashed line: $\mathcal{R} = 1 + (2/3)(\mathcal{R}_0 - 1)$; the purple dot-dashed line: $\mathcal{R} = 1 + (1/3)(\mathcal{R}_0 - 1)$; the orange solid line: $\mathcal{R} = 1$ or $U_{33} = U_{11}$. Top panel: zinc and the bottom panel: cadmium. A weak increase in V_{zz} with T (orange solid line in Cd) is discussed in Sec. III C.

(upper panel). It turns out that, if $\mathcal{R} = 1$ [i.e., $U_{33}(T) = U_{11}(T)$], there is virtually no temperature decrease in the EFG, although we have kept the average value of mean-square displacements,

$$U_{av} = (2U_{11} + U_{33})/3 \qquad (35)$$

growing with T according to experimental data [21]. It is worth mentioning that the experimental behavior of U_{33}/U_{11} in Zn is highly nonlinear in contrast to the simple linear increase in the lattice constant ratio c/a [21]. On the other hand, in the harmonic approximation, U_{33}/U_{11} should be almost independent of T, at least, for $T > T_D \sim 200$ K [43]. Therefore, in the T dependence of U_{33}/U_{11} and, consequently,

of the EFG, there is a substantial anharmonic contribution. In particular, the anharmonic effect is responsible for the negative curvature of V_{zz} in contrast to the approximate linear dependence of the harmonic model, Fig. 6.

Note, that, even at zero temperature, the value of the EFG is slightly reduced because of the zero-point vibrations. The calculated reduction is 0.6% with the mean-square displacements from Ref. [21] and 1% according to DFPT-QE. The refined calculated absolute value of the EFG is $V_{zz} = 3.51 \times 10^{21}$ V/m², the corrected for the zero-point vibrations [21] $- V_{zz} = 3.49 \times 10^{21}$ V/m². It corresponds to the quadrupole frequency 10.53 MHz for $Q(\text{Zn}) = 0.125$ b [14] and 12.64 MHz for $Q(\text{Zn}) = 0.15$ b, which compares well with the experimental value of 12.34 MHz at 4.2 K [51].

B. Cadmium

Results for cadmium are given in Figs. 8 and 9. As for the zinc calculation, we observe that the mean-square displacements U_{33} are overestimated by the DFPT-QE calculations. In addition, DFPT-QE values of U_{11} are underestimated in comparison with other models. Both effects lead to a fast decrease in V_{zz} with temperature, although, in the region of 260–360 K, the DFPT-QE harmonic treatment gives the correct slope for the V_{zz} decrease. As for zinc, our calculations of the temperature evolution of V_{zz} in Cd have turned out to be very sensitive to values of mean-square displacements U_{11} and U_{33}, especially to $\mathcal{R} = U_{33}/U_{11}$. It is worth noting that, with the mean-square values obtained by Torumba *et al.* [16] with the PHONON program [52], we have obtained reduced EFGs which compare well with the experimental results of Ref. [18] at 280 and 430 K, Fig. 8. However, our calculations also show that these values of U_{11} and U_{33} somewhat underestimate the reduction of V_{zz} at 430 K and especially at 570 K (not shown in Fig. 8). We believe that this is related to the softening of the Cd lattice [43] and increase in the ratio of $\mathcal{R}$ with temperature which lies beyond the harmonic approximation. In fact, as we know from experimentally deduced values of U_{11} and U_{33} [21], both effects are clearly present in the case of the Zn lattice, Fig. 4. Since, at the moment, there are no experimental data for the mean-square displacements of cadmium, we have performed a number of model calculations, Fig. 9. The averaged mean-square displacement $U_{av} = (2U_{11} + U_{33})/3$ has been calculated within the Debye lattice model with a temperature-dependent Debye temperature T_D. The lattice softening has been modeled by a linear decrease in T_D from 140 K (at $T = 0$ K) to 115 K (at $T = 500$ K) with the averaged value of $T_D^{av} = 127.5$ K. [This value is very close to $T_D = 131 \pm 7$ K given in Ref. [47] for Cd.] In addition, we consider an anharmonic effect modeled by a linear change in $\mathcal{R}$ from 1.5 (at $T = 0$ K) to 2.7 (at $T = 500$ K) with the averaged value of $\mathcal{R} = 2.1$. Correspondingly, we have performed four model calculations shown in Fig. 9: (1) with the lattice softening and the temperature increase in $\mathcal{R}$ (black curve in Fig. 9), (2) without softening and with $\mathcal{R}$ fixed (yellow curve), (3) with the softening and $\mathcal{R}$ fixed (blue dotted line), and (4) without softening and with $\mathcal{R}$ increased (dashed green line). The results clearly demonstrate that the best fit is achieved with the lattice softening and
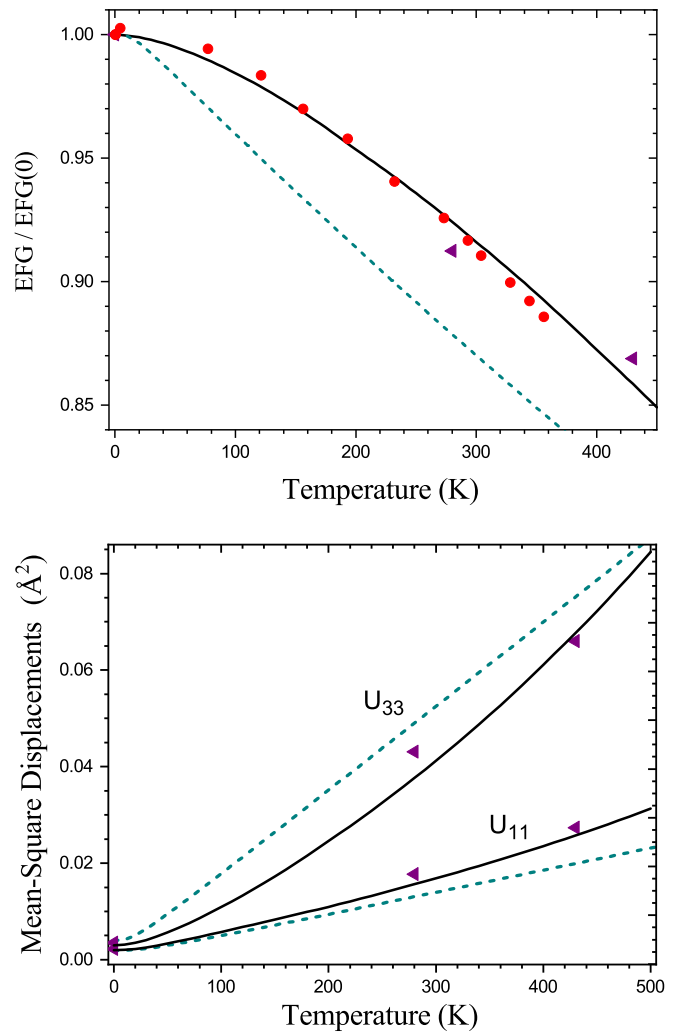

FIG. 8. Temperature evolution of V_{zz} in Cd (upper panel) determined by the mean-square displacements U_{11} and U_{33} (lower panel). The red circles stand for experimental measurements [18]; the black line: for a present model calculation taking into account softening of the lattice and an increase in U_{33}/U_{11} with T (see the text for details); the dark cyan dashed line: DFPT-QE calculations [41,42]. The purple triangles are our calculations with mean-square displacements of Table II of Ref. [16] (the PHONON code [52] within the harmonic approximation).

the temperature increase in $\mathcal{R}$ with T, whereas other models deviate from the experimental data at elevated temperatures. Although these arguments cannot be considered as a solid proof, the important finding is that both unharmonic effects improve the comparison with the experiment.

The calculated absolute value of the EFG is $V_{zz} = 7.82 \times 10^{21}$ V/m². The zero-point vibration contribution to V_{zz} amounts to 0.8% according to DFPT-QE and 0.4% in the model (1). The corrected for the zero-point vibrations value [model (1)] is $V_{zz} = 7.79 \times 10^{21}$ V/m², which corresponds to $\nu_Q = 120.7$ MHz (adopting $Q(\text{Cd}) = 0.641$ b [14]) or $\nu_Q = 143.1$ MHz (with $Q(\text{Cd}) = 0.76$ b [13]). Extrapolated to $T = 0$ quadrupole frequency in metallic cadmium is 136.9 MHz [18].
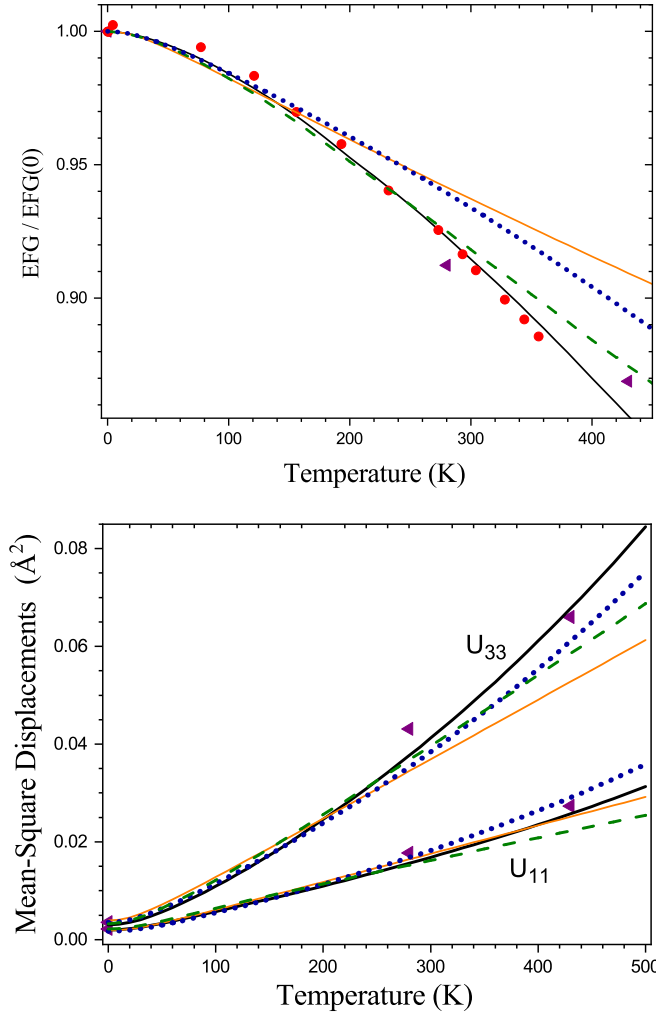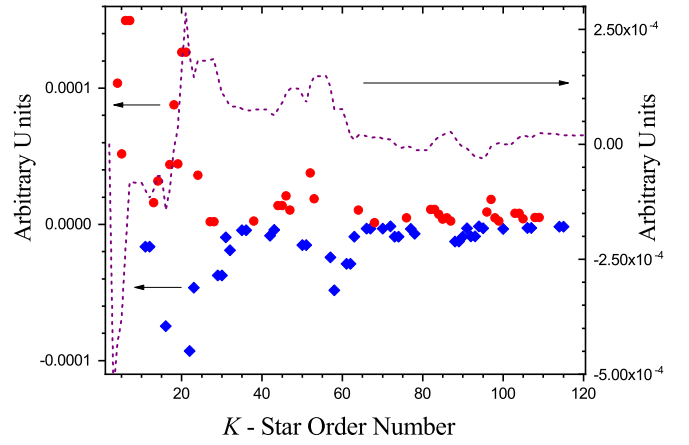
FIG. 10. Individual K-star contributions to electric-field gradient at $T = 300$ K [each term $\propto -j_2(KR_{MT})S_Q(\hat{K})(\langle\rho(\vec{K})\rangle_{T=300} - \langle\rho(\vec{K})\rangle_{T=0}$, Eq. (23)]. The blue diamonds: negative contributions; the red circles: positive contributions; the dashed purpled curve: sum of all contributions up to the chosen K star. The final value of the sum (at $n \geqslant 120$) is positive, which leads to an increase in V_{zz} at 300 K.

be schematically written as

$$V_{zz}(T) \propto \langle\rho_Q\rangle = \sum[c_1\mathcal{W}_1\rho(\vec{K}_1) - c_2\mathcal{W}_2\rho(\vec{K}_2)]. \quad (36)$$

Here, the T-dependent SRDWFs are incorporated in the weight factors $\mathcal{W}_i = \exp[-W(\vec{K}_i, T)]$ and c_i, $\rho(\vec{K}_i) > 0$ ($i = 1, 2$). Both $\mathcal{W}_1$ and $\mathcal{W}_2$ reduce with T, but if $\mathcal{W}(\vec{K}_2, T)$ drops fast enough in comparison with $\mathcal{W}(\vec{K}_1, T)$, one can have a resulting increase in the expression in the square brackets of (36) and of the whole sum.

Our detailed numerical analysis for the situation is illustrated further in Fig. 10. One can see that, at $T = 300$ K, positive contributions to the gradient (red circles), although appreciably suppressed by negative contributions (blue diamonds), finally prevail, which leads to a small positive net contribution to the EFG (the $n = 120$ value of the dashed purpled curve). At $n \geqslant 120$, the positive sum value is virtually unchanged.

IV. CONCLUSIONS

We have presented a method which can describe the temperature evolution of electric-field gradient V_{zz} in metals. The consideration is based on the fact that the average value of the quadrupole component $\langle\rho_Q\rangle$ of electron density on a sphere vibrating with the nucleus Eq. (23) is changed with T. The effective reduction of each Fourier component $\rho(\vec{K})$ of density Eqs. (19)–(21) is given by the multiplier $\exp[-W(\vec{K}, T)]$ which is the square root of the usual Debye-Waller factor. The method relies on DFT calculations of electron properties and the dependence of mean-square displacements U_{11} and U_{33} on temperature. We have found that the form and pace of the temperature change in V_{zz} is very sensitive to the mean-square displacements $U_{11}(T)$, $U_{33}(T)$, and, in particular, to their ratio $U_{33}(T)/U_{11}(T)$. The model is capable of reproducing both a decrease or an increase in the EFG with temperature. The unusual mechanism of the increase in V_{zz} with T is discussed in Sec. III C.
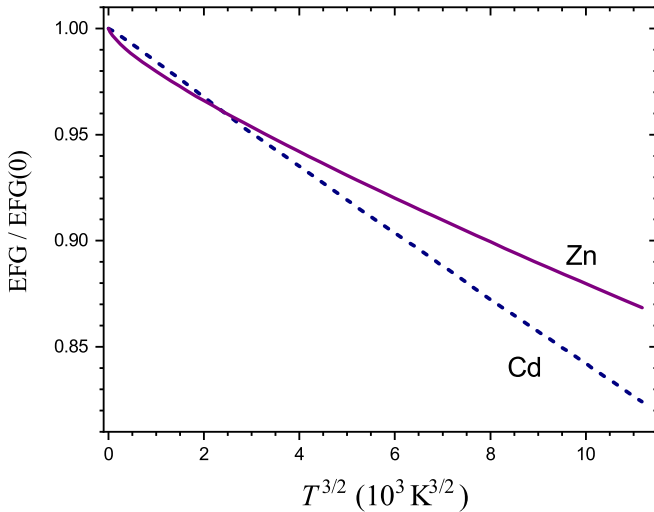

FIG. 9. Model mean-square displacements U_{11} and U_{33} in Cd (lower panel) and corresponding temperature dependencies of V_{zz} (upper panel). The red circles stand for experimental measurements [18]; the black line: for a model calculation taking into account the softening of the lattice and the increase in U_{33}/U_{11} with T. The yellow solid line: calculations without softening and the U_{33}/U_{11} ratio fixed; the blue dotted line: with the softening and the U_{33}/U_{11} ratio fixed; the green dashed line: without softening, the U_{33}/U_{11} ratio increased, see the text for details. The purple triangles are our calculations with mean-square displacements of Table II of Ref. [16].

C. Mechanism of increase in the EFG with T

The most important factor in the T dependence of the EFG is $\mathcal{R} = U_{33}/U_{11}$. As discussed in Secs. III A and III B and shown in Fig. 7, the ratio $\mathcal{R}$ has a pronounced influence on the shape of the $V_{zz}(T)$ curve. A reduction of $\mathcal{R}$ in cadmium also has an immediate and sizable effect on $V_{zz}(T)$, Fig. 7. Interestingly, for $\mathcal{R} = 1$ [$U_{11} = U_{33}$], we observe in cadmium a rare effect of a weak increase in V_{zz} with T (orange plot in Fig. 7). At first sight, this seems incompatible with the apparent reduction of $\langle\rho_Q\rangle$, Eq. (23), caused by $\exp(-W)$. Note, however, that in the sum on the right-hand side of Eq. (23), individual contributions proportional to $j_2(KR_{MT})S_Q(\hat{K})\langle\rho(\vec{K})\rangle$ are of different signs. Two such principal groups of terms can

FIG. 11. Plots of the T dependence of electric-field gradient $V_{zz}(T)/V_{zz}(T=0)$ for Zn and Cd as functions of $T^{3/2}$.

We have applied our method to hexagonal-close-packed structures of pristine zinc and cadmium. In the case of zinc where the mean-square displacements $U_{11}(T)$ and $U_{33}(T)$ are known experimentally from single-crystal x-ray diffraction [21], we obtain a very good description of the temperature change in the EFG, Fig. 6. In the case of cadmium, the behavior of $V_{zz}(T)$, Fig. 8, can be reproduced by assuming two anharmonic effects: the lattice softening (modeled by a decrease in the Debye temperature T_D with T), and an increase in the ratio U_{33}/U_{11} with T. It is worth noting that both anharmonic effects are also present in zinc [21,43].

In addition, we have performed calculations of the mean-square displacements in Zn and Cd in the harmonic approximation by using the DF perturbation treatment of the QE package [41,42]. For both metals, an approximately linear dependence in T for $U_{11}(T)$ and $U_{33}(T)$ (at $T > 40$ K) and, consequently, for the calculated V_{zz} curves has been found. In the case of cadmium, the decrease in the EFG has been exaggerated which can be accounted for by an uncertainty related to its core pseudopotential [48,49]. Using the mean-square displacements calculated at $T = 280$ and 430 K by Torumba *et al.* [16] with the package PHONON [52], we have obtained reduced values of the EFG which lie not far from the experimental data.

In our studies, we have not found an intrinsic mechanism for the $T^{3/2}$ dependence of the EFG, Eq. (2). Nevertheless, the $T^{3/2}$ plots, Fig. 11, indicate that an approximate $T^{3/2}$ law for Zn and Cd holds. For Cd, the dependence is almost perfect, for Zn, it deviates from $T^{3/2}$ at low temperatures which can be partially explained by the fact that the experimental data for mean-square displacements [21] are available only for $T > 40$ K. In any case, even experimental data for the EFG of Zn and Cd deviate from the $T^{3/2}$ law at low temperatures [20]. We, therefore, conclude that the mechanism of the temperature dependence of V_{zz} in Zn and Cd is complex

with a substantial contribution from anharmonic effects. An approximate correspondence with the $T^{3/2}$ dependence is probably due to the T behavior of SRDW factors $\exp(-W)$ [22].

Finally, we mention that, even at zero temperature, the measured EFGs are smaller than V_{zz} calculated by *ab initio* methods. The zero-temperature reduction, however, is small: 0.6% in Zn and 0.4% in Cd.

APPENDIX: QUADRUPOLAR POTENTIAL AND THE TENSOR OF THE EFG

The asymptotic behavior of the potential close to the nucleus, Eq. (25), can be understood from the two-center expansion of the Coulomb potential in double multipolar series,

$$\frac{1}{|\vec{R}(\vec{n}) - \vec{R}'(\vec{n}')|} = \sum_{\Lambda\Lambda'} v_{\Lambda\Lambda'}(\vec{n}, \vec{n}'; r, r') S_\Lambda[\hat{r}(\vec{n})] S_{\Lambda'}[\hat{r}'(\vec{n}')],$$
(A1)

where the interaction strength $v_{\Lambda\Lambda'}$ is given by [56]

$$v_{\Lambda\Lambda'}(\vec{n}, \vec{n}'; r, r') \sim \frac{(r)^l (r')^{l'}}{|\vec{X}(\vec{n}) - \vec{X}(\vec{n}')|^{l+l'+1}}.$$
(A2)

Here, $\vec{R}(\vec{n}) = \vec{X}(\vec{n}) + \vec{r}(\vec{n})$ is the radius vector close to the crystal site $\vec{n}$. For $r \ll 1$, we arrive at Eq. (25) which holds both for the contributions from the electron density around the site $\vec{n}$ and the contributions from the densities on the other sites $\vec{n}' \neq \vec{n}$.

As follows from Eqs. (24) and (25), the quadrupolar component of the potential for the hexagonal lattice can be written as

$$V_Q(r, \theta, \phi) = v_Q r^2 Y_{l=2}^{m=0}(\theta, \phi) = v_Q \frac{1}{4}\sqrt{\frac{5}{\pi}}(3z^2 - r^2). \quad \text{(A3)}$$

[We recall that, here, $v_Q = v_{(2,1)}$ is a constant.] From this relation, we obtain that the tensor of the EFG is diagonal in the Cartesian system of axis and

$$V_{zz} = \frac{\partial^2 V_Q}{\partial z^2} = \sqrt{\frac{5}{\pi}} v_Q,$$
(A4)

$$V_{xx} = \frac{\partial^2 V_Q}{\partial x^2} = \frac{\partial^2 V_Q}{\partial y^2} = -\frac{1}{2}\sqrt{\frac{5}{\pi}} v_Q.$$
(A5)

[1] E. N. Kaufmann and R. J. Vianden, Rev. Mod. Phys. **51**, 161 (1979).

[2] T. P. Das and P. C. Schmidt, Z. Naturforsch. **41a**, 47 (1986).

[3] H. Haas, Hyperfine Interact. **129**, 493 (2000).

[4] *Handbook of Applied Solid State Spectroscopy*, edited by D. R. Vij (Springer-Verlag, New York, (2006).

[5] T. Wichert and E. Recknagel, in *Microscopic Methods in Metals*, edited by U. Gonser, Topics in Current Physics, Vol. 40 (Springer-Verlag, Berlin/Heidelberg, 1986), pp. 317–364.

[6] J. Schell, P. Schaaf, and D. C. Lupascu, AIP Adv. **7**, 105017 (2017).

[7] L. Hemmingsen, K. N. Sas, and E. Danielsen, Chem. Rev. **104**, 4027 (2004).

[8] R. Dogra, A. P. Byrne, and M. C. Ridgway, J. Electron. Mater. **38**, 623 (2009).

[9] A. V. Tsvyashchenko, D. A. Salamatin, V. A. Sidorov, A. E. Petrova, L. N. Fomicheva, S. E. Kichanov, A. V. Salamatin, A. Velichkov, D. R. Kozlenko, A. V. Nikolaev, G. K. Ryasny, O. L. Makarova, D. Menzel, and M. Budzynski, Phys. Rev. B **92**, 104426 (2015).

[10] P. Blaha, K. Schwarz, and P. Herzig, Phys. Rev. Lett. **54**, 1192 (1985).

[11] P. Blaha, K. Schwarz, and P. H. Dederichs, Phys. Rev. B **37**, 2792 (1988).

[12] H. M. Petrilli, P. E. Blöchl, P. Blaha, and K. Schwarz, Phys. Rev. B **57**, 14690 (1998).

[13] L. Errico, K. Lejaeghere, J. Runco, S. N. Mishra, M. Renteria, and S. Cottenier, J. Phys. Chem. C **120**, 23111 (2016).

[14] H. Haas, S. P. A. Sauer, L. Hemmingsen, V. Kellö, and P. W. Zhao, Europhys. Lett. **117**, 62001 (2017).

[15] S.-U. Weber, T. M. Gesing, G. Eckold, R. X. Fischer, F.-J. Litterst, and K.-D. Becker, J. Phys. Chem. Solids **75**, 416 (2014).

[16] D. Torumba, K. Parlinski, M. Rots, and S. Cottenier, Phys. Rev. B **74**, 144304 (2006).

[17] A. V. Nikolaev, D. Lamoen, and B. Partoens, J. Chem. Phys. **145**, 014101 (2016).

[18] J. Christiansen, P. Heubes, R. Keitel, W. Klinger, W. Loeffler, W. Sandner, and W. Withhuhn, Z. Phys. B **24**, 177 (1976).

[19] P. Heubes, G. Hempel, H. Ingwersen, R. Keitel, W. Klinger, W. Loeffler, and W. Witthuhn, in *International Conference on Hyperfine Interactions Studied in Nuclear Reactions and Decay, Uppsala, Sweden, 1974*, edited by E. Karlsson and R. Wappling (University of Uppsala, Sweden, 1974), p. 208.

[20] H. C. Verma and G. N. Rao, Hyperfine Interact. **15**, 207 (1983).

[21] J. Nuss, U. Wedig, A. Kirfel, and M. Jansen, Z. Anorg. Allg. Chem. **636**, 309 (2010).

[22] P. Jena, Phys. Rev. Lett. **36**, 418 (1976).

[23] P. Jena, Phys. Rev. B **17**, 1046 (1978)

[24] K. Nishiyama, F. Dimmling, T. Kornrumpf, and D. Riegel, Phys. Rev. Lett. **37**, 357 (1976).

[25] D. R. Torgeson and F. Borsa, Phys. Rev. Lett. **37**, 956 (1976).

[26] M. D. Thompson, P. C. Pattnaik, and T. P. Das, Phys. Rev. B **18**, 5402 (1978).

[27] R. E. Watson, A. C. Gossard, and Y. Yaffet, Phys. Rev. **140**, A375 (1965).

[28] R. V. Kasowski, Phys. Rev. **187**, 891 (1969).

[29] P. Brüesch, *Phonons: Theory and Experiments II* (Springer-Verlag, Berlin/Heidelberg, 1986).

[30] C. Sena, M. S. Costa, G. A. Cabrera-Pasca, R. N. Saxena, and A. W. Carbonari, Hyperfine Interact. **221**, 105 (2013).

[31] T. Butz and R. Vianden, Hyperfine Interact. **221**, 99 (2013).

[32] T. Butz, Hyperfine Interact. **198**, 161 (2011).

[33] H. Bayer, Z. Phys. **130**, 227 (1951).

[34] T. Kushida, G. B. Benedek, and N. Bloembergen, Phys. Rev. **104**, 1364 (1956).

[35] D. J. Singh and L. Nordström, *Planewaves, Pseudopotentials, and the LAPW Method*, 2nd ed. (Springer, New York, 2006).

[36] C. J. Bradley and A. P. Cracknell, *The Mathematical Theory of Symmetry in Solids*, (Clarendon, Oxford, 1972).

[37] L. D. Landau and E. M. Lifshitz, *Quantum Mechanics - Nonrelativistic theory* (Pergamon, Bristol, 1995), Vol. 3.

[38] A. V. Nikolaev and P. N. Dyachkov, Int. J. Quant. Chem. **89**, 57 (2002).

[39] R. J. Glauber, Phys. Rev. **98**, 1692 (1955).

[40] P. Blaha, K. Schwarz, G. Madsen, D. Kvasnicka, and J. Luitz, J. Luitz, WIEN2K: *An Augmented Plane Wave plus Local Orbitals Program for Calculating Crystal Properties* (Vienna University of Technology, Austria, 2001).

[41] P. Giannozzi, S. Baroni, N. Bonini, M. Calandra, R. Car, C. Cavazzoni, D. Ceresoli, G. L. Chiarotti, M. Cococcioni, I. Dabo, A. Dal Corso, S. Fabris, G. Fratesi, S. de Gironcoli, R. Gebauer, U. Gerstmann, C. Gougoussis, A. Kokalj, M. Lazzeri, L. Martin-Samos, N. Marzari, F. Mauri, R. Mazzarello, S. Paolini, A. Pasquarello, L. Paulatto, C. Sbraccia, S. Scandolo, G. Sclauzero, A. P. Seitsonen, A. Smogunov, P. Umari, and R. M. Wentzcovitch, J. Phys.: Condens. Matter **21**, 395502 (2009).

[42] P. Giannozzi, O. Andreussi, T. Brumme, O. Bunau, M. Buongiorno Nardelli, M. Calandra, R. Car, C. Cavazzoni, D. Ceresoli, M. Cococcioni, N. Colonna, I. Carnimeo, A. Dal Corso, S. de Gironcoli, P. Delugas, R. A. DiStasio Jr., A. Ferretti, A. Floris, G. Fratesi, G. Fugallo, R. Gebauer, U. Gerstmann, F. Giustino, T. Gorni, J. Jia, M. Kawamura, H.-Y. Ko, A. Kokalj, E. Küçükbenli, M. Lazzeri, M. Marsili, N. Marzari, F. Mauri, N. L. Nguyen, H.-V. Nguyen, A. Oterode-la-Roza, L. Paulatto, S. Poncé, D. Rocca, R. Sabatini, B. Santra, M. Schlipf, A. P. Seitsonen, A. Smogunov, I. Timrov, T. Thonhauser, P. Umari, N. Vast, X. Wu, and S. Baroni, J. Phys.: Condens. Matter **29**, 465901 (2017).

[43] E. F. Skelton and J. L. Katz, Phys. Rev. **171**, 801 (1968).

[44] L.-M. Peng, G. Ren, S. L. Dudarev, and M. J. Whelan, Acta Crystallogr., Sect. A: Found Crystallogr. **52**, 456 (1996).

[45] G. Lehmann and M. Taut, Phys. Status Solidi B **54**, 469 (1972).

[46] J. P. Perdew, K. Burke, and M. Ernzerhof, Phys. Rev. Lett. **77**, 3865 (1996).

[47] N. G. Krishna and D. B. Sirdeshmukh, Acta Cryst. A **54**, 513 (1998).

[48] G. Prandini, A. Marrazzo, I. E. Castelli, N. Mounet, and N. Marzari, npj Comput. Mater. **4**, 72 (2018).

[49] K. Lejaeghere *et al.*, Science **351**, aad3000 (2016).

[50] H. Bertschat, E. Recknagel, and B. Spellmeyer, Phys. Rev. Lett. **32**, 18 (1974).

[51] W. Potzel, T. Obenhuber, A. Forster, and G. M. Kalvius, Hyperfine Interact. **12**, 135 (1982).

[52] K. Parlinski, Software PHONON (2003).

[53] http://ckp.nrcki.ru/

[54] http://www.jscc.ru

[55] http://parallel.uran.ru

[56] H. Yasuda and T. Yamamoto, Prog. Theor. Phys. **45**, 1458 (1971); R. Heid, Phys. Rev. B **47**, 15912 (1993).